1-26-2007

Low-energy electron collisions with CH_3Br: the dependence of elastic scattering, vibrational excitation, and dissociative attachment on the initial vibrational energy

M. Braun
Fachbereich Physik, Technische Universität Kaiserslautern, D-67653 Kaiserslautern, Germany

Ilya I. Fabrikant
University of Nebraska-Lincoln, ifabrikant@unl.edu

M-W. Ruf
University of Nebraska-Lincoln

H. Hotop
University of Nebraska-Lincoln

Published in *Journal of Physics B: Atomic, Molecular and Optical Physics* **40** (2007), pp. 659–674; doi:10.1088/0953-4075/40/4/002 Online at http://stacks.iop.org/JPhysB/40/659

Submitted November 15, 2006; revised December 7, 2006; published January 26, 2007.

Low-energy electron collisions with CH_3Br: the dependence of elastic scattering, vibrational excitation, and dissociative attachment on the initial vibrational energy

M. Braun[1], I. I. Fabrikant[1,2], M-W. Ruf[1], and H. Hotop[1]

[1] Fachbereich Physik, Technische Universität Kaiserslautern, D-67653 Kaiserslautern, Germany

[2] Department of Physics and Astronomy, University of Nebraska–Lincoln, Lincoln, NE 68588-0111, USA

Abstract

Using the laser photoelectron attachment (LPA) method at an energy width of 1–2 meV, the Br^- yield due to dissociative electron attachment to the molecule CH_3Br has been measured over the energy range 1–180 meV at a gas temperature of 600 K. The data clearly exhibit the vibrational Feshbach resonance predicted by Wilde *et al.* (2000 *J. Phys. B*: *At. Mol. Opt. Phys.* 33 5479) and associated with the $v_3 = 4$ vibrational level of the C–Br stretch mode in the neutral molecule. We also report the dependence of the rate coefficient for Rydberg electron attachment (measured at high principal quantum numbers $n \approx 150$) on gas temperature and find an Arrhenius-type behavior compatible with the results of *R*-matrix calculations and with earlier findings of electron swarm experiments. With the aim to stimulate experiments, we report absolute cross sections for elastic scattering and vibrationally inelastic scattering involving the C–Br stretch mode v_3 of CH_3Br for several initial vibrational levels in the range $v_3 = 0$–4; they were obtained with *R*-matrix calculations based on the same potential input as that involved in the computations of the cross sections for dissociative attachment.

1. Introduction

Attachment of low-energy electrons to molecules is an important process in gaseous dielectrics [1] and other environments including excimer lasers [2], discharges used for etching [3, 4], and the earth's atmosphere [5]. Due to the high electron affinity of halogen atoms *Y*, dissociative electron attachment (DEA) to halogen containing molecules *XY* (short notation Y^-/XY)

$$e^-(E) + XY \rightarrow XY^{-*} \rightarrow X + Y^- \qquad (1)$$

may often occur with large cross sections $\sigma_a(E)$ down to zero electron energy, thus effi-

ciently producing halogen anions as well as halogen atoms or halogen containing radicals which are important precursors for further reactions. Following its formation, the excited, temporary anion XY^{-*} can either decay by autodetachment (corresponding to elastic or inelastic electron scattering) or it may dissociate, thereby forming stable negative ions Y^-. For molecules (such as HF and CH_3I) which exhibit sufficiently strong long-range attraction with the colliding electrons (e.g. by the combined polarization and dipolar forces) the DEA process may be mediated and substantially enhanced by vibrational Feshbach resonances (VFRs) [6–14]. VFRs represent special scattering resonances $XY(v \geq 1)^{-*}$, with the electron weakly bound to vibrationally excited levels $XY(v \geq 1)$ of the neutral molecule. Very sharp VFRs have been observed for anion formation due to attachment of electrons to molecular clusters [14, 15]. Moreover, VFRs play an important role in the annihilation of low-energy positrons colliding with molecules [16].

VFRs involving dipolar molecules were predicted by Domcke and Cederbaum [6] as well as by Gauyacq and Herzenberg [7] and first observed in vibrationally inelastic electron scattering experiments from HF [8] (see also [12]). In DEA, VFRs have so far been observed for CH_3I [9], CH_2Br_2 [11], N_2O[13] and for molecular clusters [14, 15]. In a detailed theoretical study of DEA to the methyl halide molecules, Wilde *et al.* [10] predicted that apart from the VFR in CH_3I (attached to the C–I stretch vibrational level $v_3 = 1$) the molecule CH_3Br also exhibits a VFR, attached to the C–Br stretch level $v_3 = 4$. This prediction relies on the quality of the anion potential curve and the associated location of the crossing point of the anion curve with the neutral potential energy curve along the C–Br stretch coordinate. As compared to CH_3I ($\mu = 0.638$ au = 1.62 Debye, $\alpha = 54$ au at the equilibrium geometry [9]), the long-range electron–CH_3Br interaction (which is crucial for formation of the VFR) is characterized by a larger (supercritical) electric dipole moment μ and a smaller polarizability α ($\mu = 0.717$ au = 1.82 Debye, $\alpha = 37.3$ au [17]).

In this paper, we report the first highly resolved DEA experiment on the CH_3Br molecule. In section 2, we briefly describe the *R*-matrix approach and summarize the input for the calculations; we present calculated DEA cross sections for different initial vibrational levels CH_3Br ($v_3 = 0$–9) as well as absolute cross sections for vibrational excitation (VE) and angle-differential elastic scattering. In section 3, we describe the experimental setup and some test measurements. In section 4 we present the measured relative cross section for Br^- formation due to free electron attachment to CH_3Br molecules in a supersonic beam (nozzle temperature 600 K) and the temperature dependence for Br^- production due to Rydberg electron attachment. The experimental data confirm the predicted VFR and thus the validity of the theoretical model.

2. Calculation of absolute cross sections for dissociative electron attachment and for vibrational excitation involving CH_3Br ($v_3 \geq 0$)

2.1. R-matrix theory and calculational procedure

Dissociative electron attachment to the CH_3Br molecule in the low-energy region proceeds through electron capture into the lowest unoccupied molecular orbital of a1 symmetry. To calculate cross sections for DEA and for VE, we employ the resonance *R*-matrix theory in the approximation of one isolated resonance, as reviewed by Lane and Thomas [18]. The *R*-matrix in the fixed-nuclei approximation has the form

$$R(\rho) = \gamma^2(\rho)/[W(\rho) - E] + R_b, \tag{2}$$

where ρ is the C–Br distance relative to the equilibrium separation in the neutral molecule, $W(\rho)$ is the lowest *R*-matrix pole, $\gamma(\rho)$ is the surface amplitude and R_b is a background term

independent of ρ and electron energy E. The relation between the surface amplitude γ and the resonance width Γ is given in [18]; basically Γ is proportional to γ^2. The physical significance of $W(\rho)$ is that it represents the energy of the resonance state. Although the energy of the diabatic state of the Fano resonance theory is not exactly the same as the position of the R-matrix pole, the difference is usually small, and the diabatic anion potential $U(\rho)$ can be written as

$$U(\rho) = W(\rho) + V(\rho), \tag{3}$$

where $V(\rho)$ denotes the potential energy of the neutral molecule. The surface amplitude γ is typically a slowly varying function of ρ and can be considered as a constant. However, to introduce more flexibility in the theory, we parameterize it in the following form:

$$\gamma(\rho) = \gamma_1/[\exp(\zeta\rho) + \eta]. \tag{4}$$

In our previous work on DEA to the methyl halides [10], the parameters γ_1, ζ and η have been adjusted semiempirically to provide a realistic description of the thermal rate coefficients which are known to depend strongly on the electron and the gas temperature.

Other input of the R-matrix theory includes the potential energy curve $V(\rho)$ of the neutral molecule, parameterized in the form of a Morse function:

$$V(\rho) = D_e[\exp(-a\rho) - 1]^2, \tag{5}$$

and the potential curve for the temporary negative-ion state, parameterized in the form

$$U(\rho) = B\exp(-2b\rho) - C\exp(-b\rho) + D. \tag{6}$$

We note that the R-matrix definition of the diabatic curve is different from that used in the projection operator theory [19]. In particular, the level shift

$$\Delta(\rho) = U_{ad}(\rho) - U(\rho) \tag{7}$$

is not negatively defined in the R-matrix theory. Here, $U_{ad}(\rho)$ is the adiabatic negative-ion potential curve which for distances near the equilibrium reflects the weak long-range binding of the diffuse electron.

For the case of CH_3Br, the parameters were chosen as follows [10]. For the neutral curve $V(\rho)$, the dissociation energy is experimentally known as $D_0 = 3.036(52)$ eV (at 298 K) [17]. The vibrational spacing 0–1 for the C–Br stretch vibrational mode ν_3 is known to be 75.8 meV [20, 21]; thus $D_e^{ex} = 3.074(52)$ eV. The C–Br equilibrium separation is known to be $R_e = 193.9$ pm $= 3.664\ a_0$ [17] ($a_0 = 52.9177$ pm). The anion curve was calculated in [10] using the GAMESS computational package with the Huzinaga's 21-split-valence-orbital set, augmented with standard d and diffuse sp sets and incorporating electron correlations by the MP2 method and then fitted to equation (6). The obtained asymptotic energy of the dissociated anion CH_3–Br^- is located at −0.292 eV relative to the ground vibrational level of the neutral CH_3Br molecule, which is slightly higher than the experimental value −0.328 eV, i.e. $D^{ex} = -0.290$ eV (the electron affinity of $Br(^2P_{3/2})$ is 3.3636 eV [22]).

In the actual calculations we adopted those values for the parameters which were already used in the previous work [10], namely $D_e = 0.1145$ Hartree = 3.116 eV, $a = 0.8948\ a_0^{-1}$, $\gamma_1 = 1.500$ (Hartree $\times\ a_0)^{1/2}$, $\zeta = 1.42\ a_0^{-1}$, $\eta = 2.643$, $R_b = 0.072\ a_0$, b = $1.3753 a_0^{-1}$, B = 0.09754 Hartree = 2.654 eV, $C = 0$, $D = -0.00934$ Hartree = −0.254 eV. The difference between the numbers for D_e and D from those given above is unimportant for the results of all the calculated cross sections. The potential curves are illustrated in figure 1.

To calculate DEA cross sections, we incorporate nuclear dynamics and solve basic equations of the resonance R-matrix theory in the quasiclassical approximation [23]. As part of this procedure, we calculate electron scattering wavefunctions outside the R-matrix

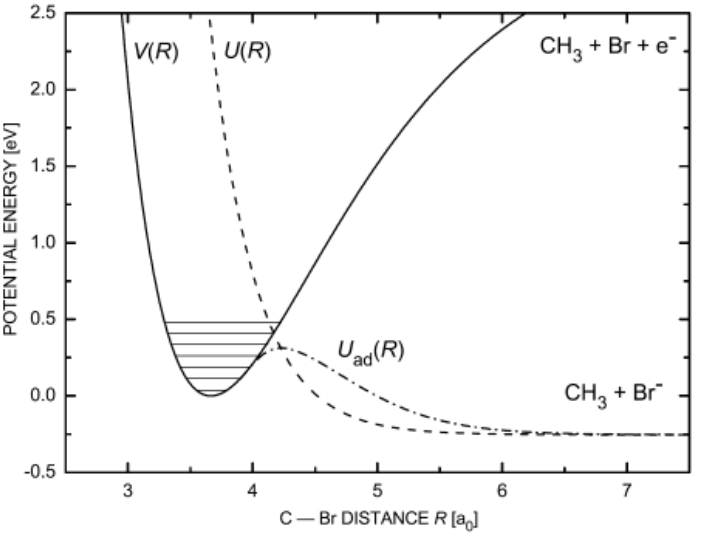

Figure 1. Potential energy curves relevant for dissociative electron attachment to CH_3Br.

sphere, which include dipolar and polarization interactions. For the electric dipole moment and the dipole polarizability of CH_3Br in the equilibrium geometry we use the values $\mu(R_e) = 1.822\ D = 0.717$ au and $\alpha(R_e) = 5.53 \times 10^{-30}\ m^3 = 37.3$ au, respectively [17]. For their dependence on the C–Br distance we assume the following functions:

$$\mu(R) = \mu_0(1+x)^3\left(1+\sum_{n=1}^{7} c_n x^n\right)^{-1} \tag{8a}$$

$$\alpha(R) = \alpha_0 + \alpha_1/R, \tag{8b}$$

where $x = (R - R_e)/R_e$. The form of the function $\mu(R)$ was taken from calculations in [24] for hydrogen halides. We adopted the results for HBr, however we used the correct equilibrium dipole moment μ_0 and changed the coefficient c_1 such as to reproduce the correct value of the transition dipole moment for CH_3Br $\mu_{01} = 0.0336$ au, obtained from the data on the intensities of infrared transitions [21]. The obtained value of c_1 is 1.054 as compared to the value of 2.216 for HBr. Additional calculations, using a multiconfigurational valence bond method [25], have generated a dipole moment function which is close to the model function used in the present calculations. Calculations of DEA cross sections with various dipole moment functions (keeping μ_0 fixed) showed that the results are very insensitive to c_n with $n > 1$, and even to c_1. The coefficients α_0 and α_1 were chosen to reproduce the correct polarizability at $R = R_e$ and at $R = \infty$ with $\alpha(\infty) = \alpha(H) + \alpha(Br) = 25.1$ au[17].

2.2. Cross sections for dissociative electron attachment to CH_3Br

The cross sections for DEA to CH_3Br molecules initially in the $v_3 = 0$ vibrational level are very small, especially at energies below 0.2 eV; they exhibit pointed-peak-type cusp structure, reflecting virtual states at the $v_3 = 1$, 2, and 3 vibrational thresholds, and a clear rounded-peak-type VFR at E = 294 meV, located about 5 meV below the $v_3 = 4$ onset, where the DEA cross section attains its maximum (see figure 2). At the higher vibrational thresholds $v_3 \geq 5$, downward-step structure, reflecting flux loss to VE channels, is observed.

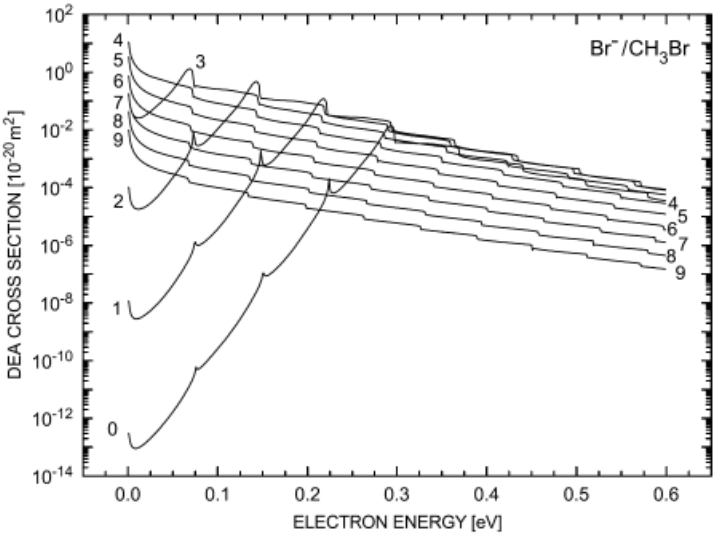

Figure 2. Absolute cross section for DEA to CH_3Br (v_3 = 0–9), E = 1–600 meV.

Analogously, these observations are also made for DEA to CH_3Br molecules initially in the v_3 = 1, 2 and 3 vibrational levels, albeit at correspondingly lower electron energies (for the VFR at 218, 143 and 69 meV, respectively) and progressively higher cross section levels.

The pronounced sharp peak observed at the v_3 = 3 threshold in DEA to CH_3Br (v_3 = 2) is also reflected in the elastic cross section for scattering from the v_3 = 2 state (see subsection 2.4). To analyze the nature of this peak, we note that the electron binding energy corresponding to the adiabatic state becomes very small at internuclear distances $\rho = R - R_e <$ 0.3 a_0, varying from 1.63 meV at ρ = 0.3 a_0 to 0.270 × 10^{-6} meV at ρ = 0 a_0. Since the right turning point for the v_3 = 2 state lies at ρ = 0.316 a_0, one can anticipate that the position of the feature in the DEA cross section for the v_3 = 2 initial state which appears near the v_3 = 3 threshold should be within 1 meV of the v_3 = 3 threshold. In fact, the DEA cross section for the v_3 = 2 initial state, calculated with a fine energy grid, peaks at E = 73.853 meV whereas the position of the v_3 = 3 threshold is located at 73.881 meV. This gives the position of the v_3 = 3 peak structure at 0.028 meV below the v_3 = 3 threshold and qualifies it as a (very narrow) VFR. It should be noted, however, that rotational motion most certainly will convert this resonance into a virtual state similar to the case of the CH_3Cl molecule [26].

Just below the v_3 = 4 threshold the DEA cross section for CH_3Br (v_3 = 2) exhibits pronounced VFR, as already mentioned above. It appears as a window resonance in the elastic cross section similar to the case of CH_3I [9]. The cross section for electron attachment to the v_3 = 3 level of CH_3Br is dominated by the VFR at 69 meV, 5 meV below the v_3 = 4 threshold. It appears as a deep window resonance in the elastic cross section for CH_3Br (v_3 = 3). For initial vibrational levels $v_3 \geq 4$, the DEA cross sections only exhibit Wigner-type downward cusp structure at the $v_3 \geq 5$ thresholds. In section 4.1, we shall present vibrationally averaged DEA cross sections appropriate for ensembles of CH_3Br molecules at the temperatures T_v = 500 and 600 K and compare them with the experimental DEA spectrum.

In all the calculations, we did not include the initial rotational distribution of the molecules. Rotational effects on DEA cross sections are usually due to the lower reaction threshold for rotationally excited states; in the present case of an exothermic DEA process we do not anticipate a significant effect due to the initial molecular rotation.

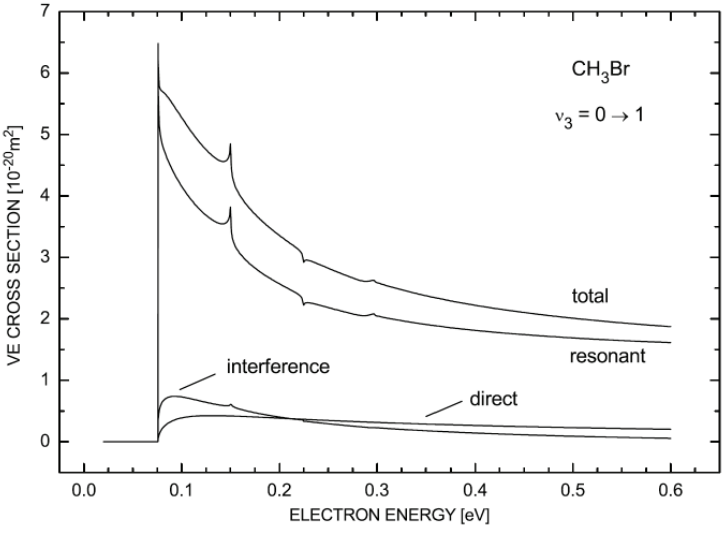

Figure 3. The resonant contribution and the total contribution (direct, resonant and interference term) to the $v_3 = 0 \rightarrow 1$ VE cross section of CH_3Br.

2.3. Cross sections for vibrational excitation of the v_3 mode of CH_3Br

Since the v_3 mode of the CH_3Br molecule is relatively strongly infrared active (as compared, say, to CF_3Br), the direct VE process can be significant and should be included, together with the resonance contribution and the interference between the direct and the resonant contribution. The calculations are based on the effective range theory approach [27], except that now for the *S*-matrix element in the lowest partial wave we use our *R*-matrix theory result. In figure 3 we present the resonant, the direct, the interference, and the total contribution to VE for the $v_3 = 0 \rightarrow 1$ process. The resonant contribution is finite at the threshold due to the supercritical dipole moment and exhibits a pronounced threshold peak. It is also interesting that the interference between the resonant and direct contribution is positive near the threshold, therefore the total cross section is greater than the simple sum of the two contributions. Note that if the resonance contribution were due to a pure s-wave, the interference term would be identically 0. However, the resonant contribution is dominated by the first dipolar angular mode that contains a significant amount of waves with higher angular momenta.

Since the VE thresholds $v_3 = 3$ and $v_3 = 4$ are associated with the virtual-state cusp and the VFR, we should anticipate much more pronounced features in VE from excited states. In figure 4 we present (angle-integrated) VE cross sections for $\Delta v = +1$ transitions from the $v_3 = 0$–4 states. Note that the cross section for the $v_3 = 0$ level was multiplied by 10. The $v_3 = 2 \rightarrow 3$ and $v_3 = 3 \rightarrow 4$ transitions are particularly interesting. First, the cross sections are very large at the threshold and not far from their unitary limit, 158×10^{-20} m^2. These are perhaps the largest vibrational excitation cross sections ever predicted. Second, we see very pronounced cusps at the $v_3 = 3$ threshold in the $v_3 = 1 \rightarrow 2$ and $v_3 = 2 \rightarrow 3$ cross sections. The influence of the VFR below the $v_3 = 4$ threshold is clearly seen in the $v_3 = 2 \rightarrow 3$ and $v_3 = 3 \rightarrow 4$ transitions. Some less pronounced features are observed at higher thresholds.

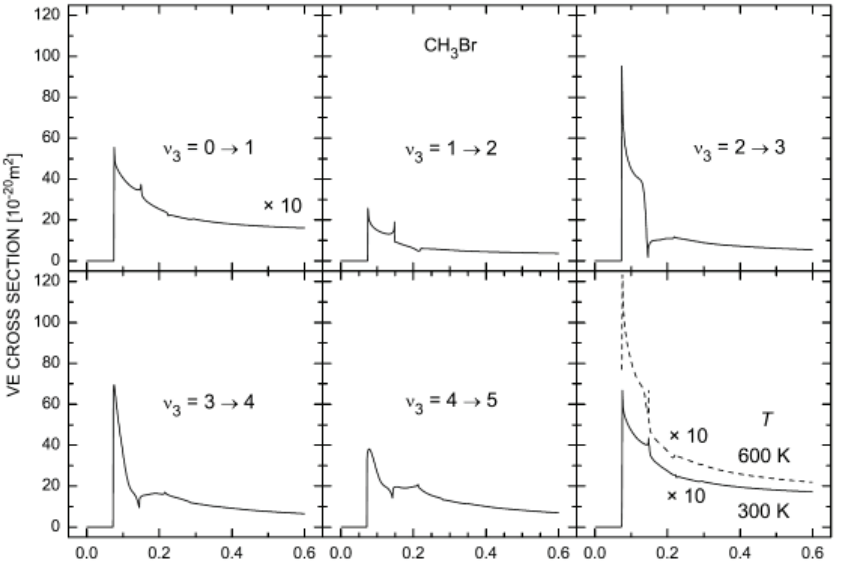

Figure 4. Calculated VE cross sections ($\Delta v = +1$) for CH_3Br in the initial vibrational states $v_3 = 0$–4 and for thermal vibrational ensembles at $T = 300$ K and $T = 600$ K.

2.4. Differential cross sections for elastic scattering from vibrationally excited states

Since very pronounced features are observed in the DEA and VE cross sections, we can anticipate their appearance in the elastic cross section as well. However, it is well known that for polar molecules the resonance features in elastic scattering can be significantly masked by the strong direct contribution. Moreover, in the approximation of a fixed molecular orientation, used in our calculations so far, the total elastic cross section is divergent. For diatomic polar molecules in Σ electronic states and asymmetric tops this divergence can be removed by inclusion of rotations for large orbital angular momenta of the incident electron (or small scattering angles) and calculation of the corresponding scattering amplitudes in the Born dipole approximation [28]. However, for symmetric top molecules, like CH_3Br, even inclusion of rotations does not average out the permanent dipole moment, and the total cross section is still divergent [29]. The reason for this is the presence of degenerate channels coupled by the dipolar interaction [30, 31]. To remove this degeneracy, the inversion splitting should be included [32], and the cross section becomes proportional to the logarithm of the inversion splitting [33]. Since the range of impact parameters contributing to the total cross section becomes enormous, we do not think that it is of much practical value to calculate the total cross sections. Therefore we calculated differential cross sections for elastic scattering from the $v_3 = 1$, 2 and 3 states for the angles 60°, 90°, 120°, 150°, and 180°. In figure 5 we show the results obtained for the angles 60° and 180° which are representative for the behavior at smaller and larger scattering angles, the latter showing a stronger decrease towards higher energies. The $v_3 = 2$ cross section is significantly affected by the $v_3 = 3$ cusp, and the $v_3 = 3$ cross section by the VFR below the $v_3 = 4$ threshold.

The calculations were carried out using the methods described in [27, 34] with some modifications incorporating the resonant scattering in the lowest partial wave and scattering by both dipolar and polarization potentials in higher partial waves [35]. More details and results will be reported in a future publication. The data in the figures of this paper will be provided in numerical form upon request.

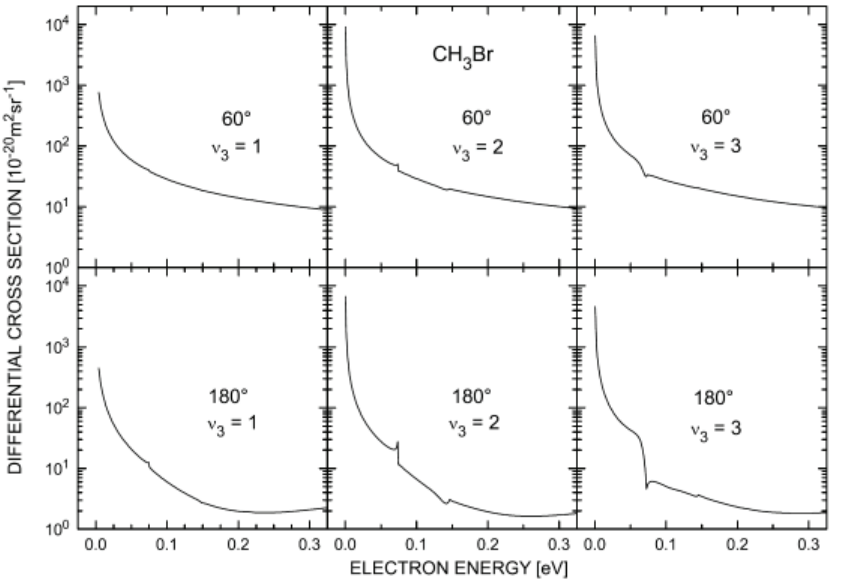

Figure 5. Differential cross section for elastic electron scattering from CH_3Br ($v_3 = 1, 2, 3$) molecules at the angles 60° and 180°.

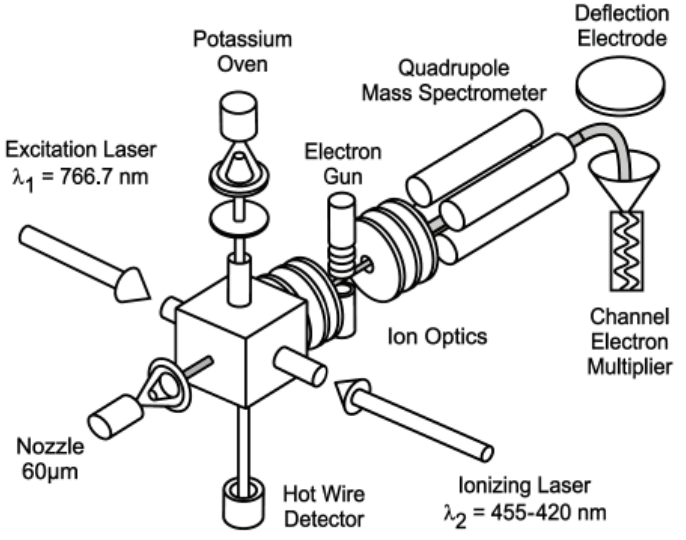

Figure 6. Experimental setup for laser photoelectron attachment studies involving a supersonic target beam.

3. Experimental setup, procedure, and tests

In the present work we use the laser photoelectron attachment (LPA) method involving a differentially pumped supersonic target beam, as illustrated in figure 6 and previously described in [36, 37]. Energy-variable, monoenergetic electrons, created by photoionization of atoms in a collimated beam, interact with the target molecules of interest in the

region where the photoionization process takes place (centre of reaction chamber RC). Negative ions due to electron attachment reactions are detected with a quadrupole mass spectrometer.

In the present LPA work, photoelectrons (current around 50 pA) are produced by two-step photoionization of potassium atoms [36–38]. Both hyperfine components of ground state $^{39}K(4s, F = 1, 2)$ atoms in a collimated beam (collimation 1:400, diameter 1.5 mm) from a doubly differentially pumped metal vapor oven are transversely excited to the $^{39}K^*(4p_{3/2}, F = 2, 3)$ states by the first sidebands of the electro-optically modulated (frequency 220.35 MHz) output of a long-term stabilized single mode cw titanium:sapphire laser ($\lambda_1 = 766.7$ nm) [39]. Part of the excited state population is transferred to high Rydberg levels (nd, (n +2)s, $n \geq 12$) or photoionized by interaction with the intracavity field of a multimode tunable dye laser (power up to 5 W), operated in the blue spectral region ($\lambda_2 = 472-424$ nm, dye Stilbene 3). The energy of the photoelectrons is continuously varied over the range 0–200 meV by tuning the wavelength of the ionizing laser ($\lambda_2 < 455$ nm). At wavelengths above 455 nm, $^{39}K^{**}(n$s, nd) Rydberg atoms are produced, used to study Rydberg electron transfer (RET) reactions of the type

$$K^{**}(nl) + CH_3Br \rightarrow K^+ + Br^- + CH_3. \tag{9}$$

Electrons, created in the overlap volume of the potassium atom beam and the laser beams, may attach to molecules in a collimated, differentially pumped supersonic beam of pure CH_3Br (provided by Air Liquide Co., stated purity > 98%), propagating in a direction perpendicular to both the potassium and the laser beams. The diameter of the target beam in the reaction region amounts to 3 mm. The nozzle diameter was $d_0 = 60\ \mu$m, the stagnation pressure fixed at $p_0 = 1$ bar, and the nozzle temperature varied over the range $T_0 = 300$–600 K.

Anions, generated by electron attachment and drifting out of the essentially field free reaction chamber, are imaged into a quadrupole mass spectrometer (m/q ≤ 2000 u/e) with a combination of two electrostatic lenses (see figure 6). The ion optics are carefully tuned for optimum detection of Br^- ions. In view of the low anion signals, the mass resolution was reduced to a level which resulted in simultaneous detection of $^{79}Br^-$ and $^{81}Br^-$ ions. The transmitted ions are accelerated to an energy of 1.5 keV and detected by a differentially pumped off-axis ceramic channel electron multiplier (Sjuts) with a very low noise level ($<0.02\ s^{-1}$).

The reaction volume is surrounded by a cubic chamber; the inner surfaces are coated with colloidal graphite. By applying bias potentials to each face of the cube, dc stray electric fields are reduced to values $F_S < 1$V m^{-1}. Magnetic fields are reduced to values ≤ 2 μT by compensation coils located outside the vacuum apparatus. The electron energy resolution is limited by the bandwidth of the ionizing laser ($\Delta E_L \approx 0.15$ meV), residual electric fields ($\Delta E_F \leq 1$–2 meV), the Doppler effect, present in both the photoionization and in the attachment process (overall Doppler width $\Delta E_D \approx 0.1E^{1/2}$, ΔE_D and E in meV), and space charge broadening E_{SC} due to K^+ photoions generated in the reaction volume ($\Delta E_{SC} \approx 0.6$ meV at 20 pA photocurrent, see figure 7 in [40]).

For diagnostics of the target beam (especially with respect to possible cluster formation and the detection of impurity species), anion mass spectra were taken using the RET reaction (9) with $K^{**}(nl)$ atoms excited to quantum numbers around $n = 150$. We note that the RET-induced anion signals are typically a factor of 100 higher than the signals due to free electron attachment at energies around $E = 10$ meV. In figure 7 we present anion mass spectra due to RET involving the supersonic CH_3Br beam at six nozzle temperatures T_0 between 300 K and 600 K. At $T_0 \leq 400$ K, the anion mass spectra are dominated by cluster anions of the type $(CH_3Br)_q\ Br^-$ ($q \geq 1$), $(CH_3Br)^-_q$ ($q \geq 2$), and $(CH_3Br)_qCH3^-$ ($q \geq 2$); the weak signal around $M = 95$ u in the upper left mass spectrum is attributed to CH_3Br^-. As

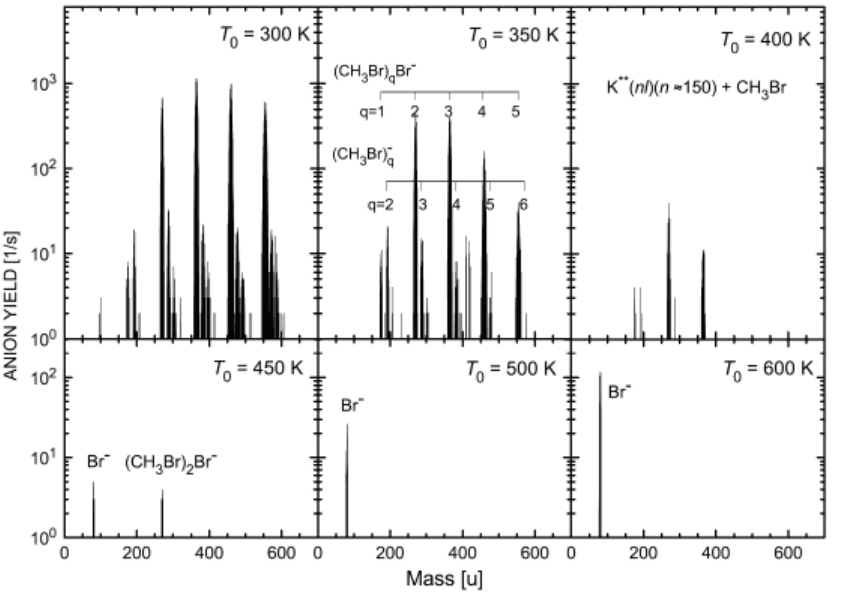

Figure 7. Anion mass spectra due to electron transfer from K(*nl*) Rydberg atoms ($n \approx 150$) to CH_3Br molecules and clusters in a supersonic beam. Pure CH_3Br gas was expanded at the fixed stagnation pressure $p_0 = 1$ bar and nozzle temperatures T_0 ranging from 300 to 600 K. These data were taken with improved mass resolution as compared to the measurements in figures 8 and 10.**

discussed in section 2 (see also [10, 41]), Br^- formation from CH_3Br molecules is characterized by an activation barrier of about 0.3 eV; thus the corresponding anion signal is expected to be weak at low temperatures, unless Br^- anions were efficiently formed by a DEA process involving neutral CH_3Br clusters, e.g. via the reaction

$$e^- + (CH_3Br)_2 \rightarrow Br^- + (CH_3Br + CH_3). \tag{10}$$

The anion mass spectra in figure 7 indicate, however, that Br^- formation due to electron attachment to neutral CH_3Br clusters is a very weak process at all temperatures and that, in particular, reaction (10) must have a very small cross section. As suggested by the relative intensities of the $(CH_3Br)_q\,Br^-$ ($q \geq 1$) and $(CH_3Br)_q^-$ ($q \geq 2$) cluster anions, the dominant reaction paths for neutral clusters with size N are dissociative attachment

$$e^- + (CH_3Br)_N \rightarrow (CH_3Br)_q\,Br^- + CH_3 \qquad (N \geq 2,\ q = N - 1) \tag{11}$$

and evaporative attachment

$$e^- + (CH_3Br)_N \rightarrow (CH_3Br)_q^- + CH_3Br \qquad (N \geq 3,\ q = N - 1). \tag{12}$$

These processes are accompanied by the minor dissociative attachment channel

$$e^- + (CH_3Br)_N \rightarrow (CH_3Br)_q\,CH_3^- + Br \qquad (N \geq 3,\ q = N - 1) \tag{13}$$

and possibly by the nondissociative process

$$e^- + (CH_3Br)_N \rightarrow (CH_3Br)_q^- \qquad (N \geq 2,\ q = N). \tag{14}$$

At temperatures above 400 K, the cluster contribution strongly decreases with rising temperature and is essentially absent at $T_0 \geq 500$ K while Br^- formation involving CH_3Br monomers strongly increases with an Arrhenius-type behavior (see section 4).

A nontrivial aspect of DEA experiments with regard to the energy dependence of the measured anion yield is the possible variation of the anion detection efficiency with the electron energy E and with the initial vibrational energy E_v of the target molecule since part of these energies E and E_v appears as kinetic energy of the recoiling anion. The anion detection efficiency is proportional to the respective fraction of all Br^- anions which recoil into the detection solid angle (as given by the solid angle of the entrance hole of the ion optics with reference to the reaction centre). For an estimate of this detection efficiency one has to know the angular and the velocity distributions of the recoiling Br^- ions. They depend on the initial vibrational level v_3 of CH_3Br, on the electron energy E, and on the nozzle temperature T_0 (which determines the velocity of the CH_3Br molecules prior to electron attachment).

In the case of DEA to CH_3Br, 15.8% of the translational excess energy is carried away by the heavier Br^- fragment. As mentioned in section 2.1, DEA to CH_3Br ($v_3 = 0$) is an exothermic process; the energy of the dissociated $CH_3 + Br^-$ system lies 328(52) meV below the vibrational ground state of CH_3Br. In DEA to CH_3Br one expects—similar to the case of CH_3I [42]—no vibrational and rotational excitation of the CH_3 fragment. Thus, zero-energy electron attachment to CH_3Br ($v_3 = 0$) molecules yields Br^- anions with a centre-of-mass kinetic energy of $W_{CM}(Br^-; E = E_v = 0) = 52$ meV. The energy $W_{CM}(Br^-)$ rises by about 12 meV with each added vibrational quantum of the v_3 vibrational mode. In the present experiment, the electron energy is varied over the range E = 0–180 meV; the corresponding variation of the CM energy of Br^- amounts to 28 meV. For CH_3Br ($v_3 = 4$), for example, the initial vibrational energy (including the effects of anharmonicity) amounts to $E(v_3 = 4) = 298$ meV and one obtains $W_{CM}(Br^-) = 99/127$ meV and $u_{CM}(Br^-) = 489/554$ m/s for $E = 0/180$ meV.

Assuming that the rotational degrees of freedom in the CH_3Br molecule are fully cooled, while the vibrational energy remains unaffected in the supersonic expansion process, the average velocity $\langle v \rangle$ of the CH_3Br molecules at the nozzle temperature T_0 is obtained from $\langle v \rangle = (8k_BT_0/M)^{1/2}$, where k_B is the Boltzmann constant and M the molecular mass [43]. For $T_0 = 300/600$ K and $M = 95$ u one obtains $\langle v \rangle = 458/648$ m s^{-1}.

The variation of the anion detection efficiency with E and Ev is estimated by a calculation of the CM solid angle for all those DEA processes for which Br^- anions recoil into the laboratory detection solid angle (cone with half angle of $\theta = 6°$ [37]). As long as the initial molecular velocity v exceeds the CM recoil velocity $u_{CM}(Br^-)$ there are two contributions due to forward (towards the ion optics) and backward dissociation of the temporary CH_3Br^- anion. The effective CM detection solid angle for these two processes is given by

$$\Omega_f[\mathrm{sr}] = \sin^2\{\theta(v + u)/(2u)\} \tag{15a}$$

$$\Omega_b[\mathrm{sr}] = \sin^2\{\theta(v - u)/(2u)\}. \tag{15b}$$

For $v \leq u$, backward dissociation is not detected, i.e. $\Omega_b(v \leq u) = 0$.

As an example, we consider the variation of the sum $\Omega_{f+b} \equiv \Omega_f + \Omega_b$ for Br^- anions resulting from RET processes (9) at high n ($E \approx 0$ eV). Inspection of the DEA cross sections in figure 2 at near-zero electron energy and of the vibrational level populations at vibrational temperatures between 300 K and 600 K shows that the RET rates are mainly determined by the contribution of the $v_3 = 4$ initial vibrational level. With the corresponding CM recoil velocity of Br^- (489 m s^{-1}) one finds an increase of the effective detection solid angle Ω_{f+b} by a factor of 1.47 when the nozzle temperature rises from 300 K to 600 K. In a similar way, we estimated the energy-dependent detection efficiency for free electron attachment at the fixed nozzle temperature $T_0 = 600$ K as a function of electron energy and of initial vibrational level v, corrected each calculated partial cross section $\sigma_v(E)$ for the cor-

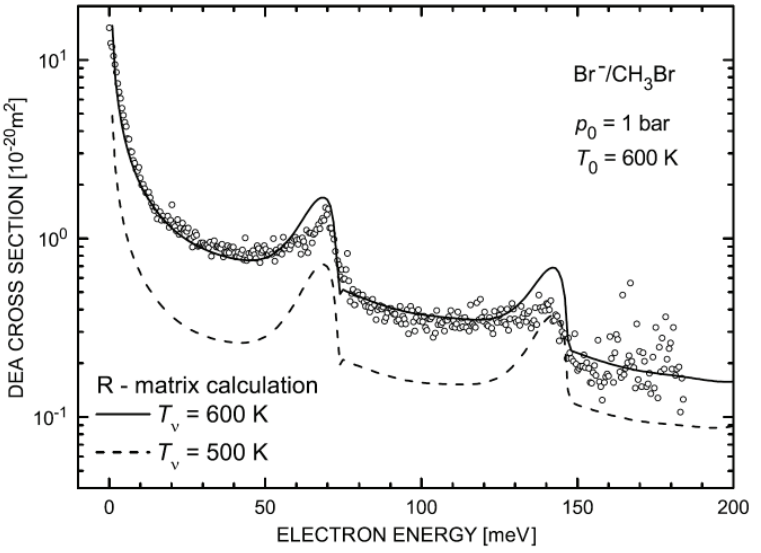

Figure 8. Measured yield (open circles) for Br^- formation in dissociative low-energy electron attachment to CH_3Br molecules (nozzle temperature T_0 = 600 K) over the electron energy range E = 1–180 meV. The full and broken curves show theoretical cross sections calculated at vibrational temperatures T_v of 600 K and 500 K, respectively. These calculated cross sections have been corrected for the (weak) dependence of the anion detection efficiency with electron energy (see section 3). The experimental data for T_0 = 600 K have been normalized to the calculated cross section for T_v = 600 K at E = 15 meV.

responding variation and used these corrected cross sections for obtaining the thermally averaged cross section for comparison with the experimental data. The detection efficiency for this averaged cross section varies only little: over the range E = 1–180 meV, it drops by 5%.

4. Experimental results for DEA to CH_3Br and comparison with theory

In the present work, two sets of experimental results have been obtained. At the fixed nozzle temperature T_0 = 600 K, we measured the yield for Br^- formation over the electron energy range 1–180 meV. These data will be presented and compared with the calculated absolute cross section in section 4.1. Moreover, we determined the variation of the rate coefficient for Rydberg electron transfer (RET) with nozzle temperature over the range T_0 = 300–600 K, as measured at high principal quantum numbers (n ≈ 150). These results will be presented and compared with the calculated temperature dependence in section 4.2, thereby shedding light on the activation energy for the investigated DEA process.

4.1. Dependence of the DEA cross section on electron energy (T_0 = 600 K)

In figure 8, we show the Br^- yield due to DEA to CH_3Br over the electron energy range 1–180 meV, as measured with pure CH_3Br gas expanded at the fixed nozzle temperature T_0 = 600 K and the stagnation pressure p_0 = 1 bar. For comparison we show an absolute DEA cross section, calculated as the thermal average for the vibrational temperature T_v = 600 K

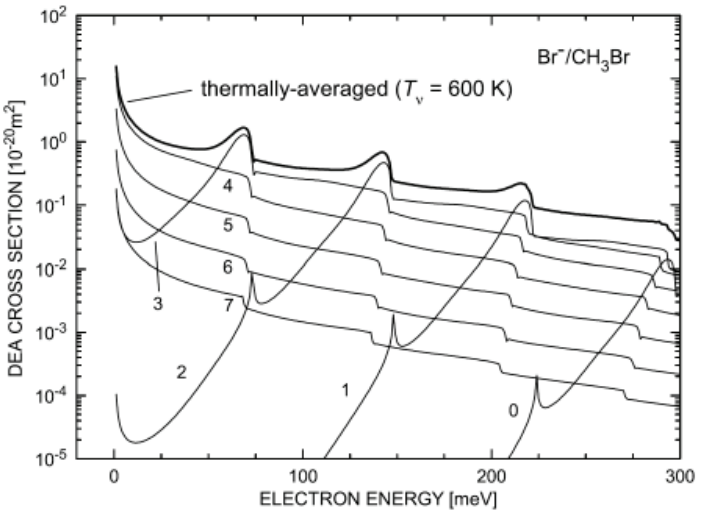

Figure 9. Population-weighted partial cross sections for $v_3 = 0–7$ and thermally averaged cross section (thick full curve) for dissociative electron attachment to CH_3Br molecules at the vibrational temperature $T_v = 600$ K.

(the weak variation of the anion detection efficiency with electron energy, described in section 3, has been included). The experimental and theoretical results are normalized to each other at $E = 15$ meV.

The most pronounced feature in both the experimental and the theoretical attachment spectrum is—apart from the strong rise towards zero electron energy due to s-wave attachment—the sharp and prominent peak at about 70 meV which is due to a VFR involving an electron loosely bound to the $v_3 = 4$ vibrational level of CH_3Br. It reflects DEA processes involving CH_3Br molecules initially in the $v_3 = 3$ level and has been predicted by Wilde *et al.* [10]. This VFR also appears in the partial attachment cross sections for molecules initially in the lower vibrational levels $v_3 = 0$, 1, and 2, but the corresponding structure shows up at higher electron energies (298, 218, and 143 meV, respectively, see also section 2.2). The calculated partial cross sections $\sigma_v(E)$for $v_3 = 0–7$ at $T_v = 600$ K, weighted with their respective population factors at $T_v = 600$ K, and the thermally averaged cross section are shown in figure 9. One observes that at electron energies below about 40 meV, CH_3Br molecules in the initial $v_3 = 4$ level provide the dominant contribution to the DEA cross section. Over the range 60–130 meV the contribution from the $v_3 = 3$ population is strongest, and from 130–200 meV that of the $v_3 = 2$ population plays the largest role.

The agreement between the measured anion yield and the calculated energy dependence in figure 8 is generally good except for the range near $E = 140$ meV in which the experimental data exhibit a feature which is weaker than the predicted VFR involving molecules initially in the $v_3 = 2$ level. This difference cannot be attributed to the possible effects of vibrational cooling in the supersonic expansion of the target beam for two reasons. (i) In order to improve the agreement with experiment one would need a weaker contribution from the $v_3 = 2$ level (relative to the $v_3 = 3$ level) in the calculated spectrum, but the reverse happens if the vibrational temperature is lowered. For illustration, we have included in figure 8 a theoretical attachment spectrum obtained for the vibrational temperature $T_v = 500$ K. (ii) It will be shown in section 4.2 that in the supersonic expansion of the pure CH_3Br beam vibrational cooling amounts to a reduction of the vibrational temperature of less than 30 K.

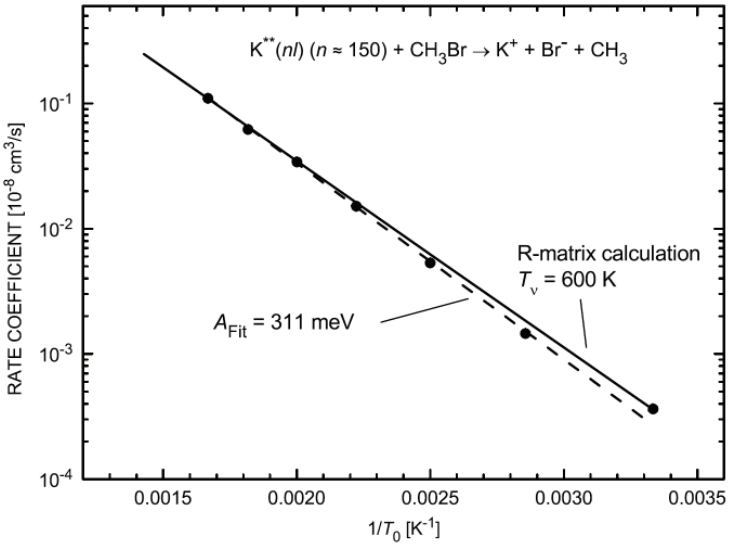

Figure 10. The temperature dependence of the rate coefficients $k_{nl}(T_0)$ for Rydberg electron transfer from K**(nl) atoms ($n \approx 150$) to CH_3Br molecules yielding Br− anions.

4.2. Temperature dependence of rate coefficient for Rydberg electron attachment

At near-zero electron energy, electron attachment to CH_3Br molecules is dominated by the contribution from the initial $v_3 = 4$ level (see figure 9). The thermal population factor of this level (relative to the $v_3 = 0$ level) ranges from 9.6×10^{-6} to 3100×10^{-6} when the vibrational temperature T_v rises from 300 K to 600 K. Thus, one expects a change of the RET rate coefficient at high n by about a factor of 300 over this temperature range. In view of the low signals for free electron attachment we limited investigations of the temperature dependence to RET measurements.

In figure 10, we present rate coefficients for the RET process (9), as measured for $n \approx 150$ and normalized to the calculated, thermally averaged absolute RET rates $\langle k_{nl}(T_v)\rangle$ at the nozzle temperature $T_0 = 600$ K. The *experimenta*l data have been corrected for the expected T_0 dependence of the anion detection efficiency (see section 3). Both the experimental and the theoretical data (obtained with the assumption $T_v = T_0$) exhibit (near) Arrhenius-type behavior given by the functional dependence

$$\langle k_{nl}(T_v)\rangle = k_0 \exp[-A/(k_B T_v)], \tag{16}$$

where A denotes the activation energy. For the theoretical results, an Arrhenius fit (16) yields the activation energy of 298 meV [10] whereas the RET data yield an activation energy of 311 meV. This (rather small) difference can be explained by a certain amount of vibrational cooling in the supersonic expansion of the CH_3Br target beam. To account for this possibility, theoretical rates were calculated for vibrational temperatures T_v reduced by a certain amount ΔT, i.e. $T_v = T_0 - \Delta T$ (using for simplicity the same value ΔT at all T_0). These calculations showed that the experimentally measured temperature dependence can be well recovered with the choice $\Delta T = 10$ K, i.e. only little vibrational cooling occurs as may be expected for our pure CH_3Br beam at $p_0 = 1$ bar and the nozzle diameter of 60 μm. We note that in studies of the temperature dependence of SF_5^- formation in electron attachment to SF_6 molecules in a *seeded* supersonic beam (12.5% SF_6 in helium carrier gas, p_0

= 1 bar, nozzle diameter 60 μm) we found a reduction of the vibrational temperature by about 100 K [44, 45].

We note that the value of the activation energy A depends on the electron energy [10] (on the energy distribution function and its average electron energy in the case of electron swarm experiments [46]). It was shown in [10], that the calculated value of A drops to 262/225 meV when the electron energy is increased to 50/100 meV. Based on calculations with Maxwellian electron ensembles (electron temperature T_e equal to the gas temperatures, i.e. $T_e = T_G = T_v \equiv T$), the value $A = 249$ meV was obtained from a fit to the calculated thermal rate coefficients $k_a(T)$ over the range $T = 300$–800 K [10]. Previous experimental studies of DEA to CH_3Br involving electron swarms with equal electron and gas temperature yielded temperature-dependent rate coefficients $k_a(T)$ which could also be well fitted by an equation of the form (16). Using a pulse sampling method ($T \approx 350$–490 K), Wentworth *et al.* [47] determined the value $A = 247(17)$ meV while Petrovic and Crompton [48], applying the Cavalleri electron density sampling technique ($T = 293$–500 K), derived the value 260(15) meV; both are in very good agreement with that obtained from the R-matrix calculations. Using the flowing afterglow Langmuir probe method ($T = 300$–585 K), Alge *et al.* [49] obtained the estimate $A = 300(60)$ meV which is also consistent with the other results. More recently, Levy *et al.* [50] used a discharge-flow system with electron cyclotron resonance detection and studied DEA to CH_3Br at four temperatures in the range $T = 293$–1022 K. From the rate coefficients for the two lower temperatures (293 K and 615 K, see table 2 in [50]), an activation energy of 238 meV is deduced which is compatible with the other values.

5. Conclusions

The measured energy dependence of the DEA cross section for Br^- formation and the measured dependence of the rate coefficient for Rydberg electron attachment on vibrational temperature of CH_3Br provide strong support for the correctness of the theoretical model for dissociative electron attachment to CH_3Br developed by Wilde *et al.* [10], especially for the location of the crossing point of the (diabatic) anion curve with the neutral potential curve. In particular, our experimental results confirm the prediction of a vibrational Feshbach resonance (attached to the $v_3 = 4$ vibrational level of CH_3Br) in DEA to CH_3Br molecules in an initial vibrational level with $v_3 \leq 3$. In order to stimulate further experimental studies and thereby allow for additional tests of the theoretical input, we calculated absolute cross sections for $\Delta v_3 = +1$ vibrational excitation of CH_3Br molecules out of several initial levels $v_3 = 0$–4 into the respective higher level and angle-differential elastic scattering cross sections. Depending on the initial vibrational level, these cross sections show more or less clear structure at the vibrational thresholds (especially at the $v_3 = 3, 4$ onsets).

Acknowledgments

This work has been supported by the Deutsche Forschungsgemeinschaft through grant Ho 427/29 and by the Forschungszentrum *Optische Technologien und Lasergesteuerte Prozesse*. We gratefully acknowledge U. Hohm for helpful comments on the dipole polarizability of methyl bromide and G. A. Gallup for communicating unpublished results. I.I.F. thanks the Fachbereich Physik at TU Kaiserslautern for their hospitality during recent stays at Kaiserslautern. I.I.F. was supported by the US National Science Foundation, grant PHY0354688.

References

[1] Christophorou L G 1984 *Electron-Molecule Interactions and their Applications* vols. 1 and 2 (New York: Academic)

[2] McDaniel E W and Nighan W L 1982 *Applied Atomic Collision Physics: Vol. 3. Gas Lasers* (New York: Academic)

[3] Manos D M and Flamm D L 1989 *Plasma Etching* (Boston: Academic)

[4] Christophorou L G and Olthoff J K 2004 *Fundamental Electron Interactions with Plasma Processing Gases* (New York: Kluwer Academic/Plenum)

[5] Wayne R P 1991 *Chemistry of Atmospheres* (Oxford: Clarendon)

[6] Domcke W and Cederbaum L S 1981 *J. Phys. B: At. Mol. Phys.* **14** 149

[7] Gauyacq J P and Herzenberg A 1982 *Phys. Rev. A* **25** 2959

[8] Knoth G, Gote M, Rädle M, Jung K, and Ehrhardt H 1989 *Phys. Rev. Lett.* **62** 1735

[9] Schramm A, Fabrikant I I, Weber J M, Leber E, Ruf M-W, and Hotop H 1999 *J. Phys. B: At. Mol. Opt. Phys.* **32** 2153

[10] Wilde R S, Gallup G A, and Fabrikant I I 2000 *J. Phys. B: At. Mol. Opt. Phys.* **33** 5479

[11] Schramm A, Ruf M-W, Stano M, Matejcik S, Fabrikant I I, and Hotop H 2002 *J. Phys. B: At. Mol. Opt. Phys.* **35** 4179

[12] Čížek M, Horćek J, Allan M, Fabrikant I I, and Domcke W 2003 *J. Phys. B: At. Mol. Opt. Phys.* **36** 2837

[13] Allan M and Skalický T *2003 J. Phys. B: At. Mol. Opt. Phys.* **36** 3397

[14] Hotop H, Ruf M-W, Allan M, and Fabrikant I I 2003 *Adv. At. Mol. Opt. Phys.* **49** 85

[15] Weber J M, Leber E, Ruf M-W, and Hotop H 1999 *Phys. Rev. Lett.* **82** 516

[16] Surko C M, Gribakin G F, and Buckman S J 2005 *J. Phys. B: At. Mol. Opt. Phys.* **38** R57

[17] Lide D R 1994–1995 *CRC Handbook of Chemistry and Physics* 76th edn. (Boca Raton, FL: CRC Press)

[18] Lane A M and Thomas R G 1958 *Rev. Mod. Phys.* **30** 257

[19] Domcke W 1991 *Phys. Rep.* **208** 97

[20] Shimanouchi T 1972 *Tables of Molecular Frequencies* vol. I (*National Standard Reference Data Series* (*NSRDS*), No. 39) (Washington, DC: National Bureau of Standards)

[21] Bishop D M and Cheung L M 1982 *J. Phys. Chem. Ref. Data* **11** 119

[22] Andersen T, Haugen H K, and Hotop H 1999 *J. Phys. Chem. Ref. Data* **28** 1511

[23] Fabrikant I I 1991 *Phys. Rev. A* **43** 3478

[24] Ogilvie J F, Rodwell W R, and Tipping R H 1980 *J. Chem. Phys.* **73** 5221

[25] Gallup G A and Fabrikant I I 2006 unpublished results

[26] Fabrikant I I and Wilde R S 1999 *J. Phys. B: At. Mol. Opt. Phys.* **32** 235

[27] Fabrikant I I 1980 *Phys. Lett. A* **77** 421

[28] Fabrikant I I 1976 *Sov. Phys.—JETP* **44** 77

[29] Crawford O H 1967 *J. Chem. Phys.* **47** 1100

[30] Engelking P C 1982 *Phys. Rev. A* **26** 740

[31] Engelking P C and Herrick D R 1984 *Phys. Rev. A* **29** 2425

[32] Herzberg G 1945 *Infrared and Raman Spectra of Polyatomic Molecules* (New York: Van Nostrand-Reinhold)

[33] Gallup G A 2006 private communication

[34] Fabrikant I I 1983 *J. Phys. B: At. Mol. Phys.* **16** 1253

[35] Fabrikant I I 1979 *J. Phys. B: At. Mol. Phys.* **12** 3599

[36] Weber J M, Leber E, Ruf M-W and Hotop H 1999 *Eur. Phys. J. D* **7** 587

[37] Ruf M-W, Barsotti S, Braun M, Fabrikant I I and Hotop H 2004 *J. Phys. B: At. Mol. Opt. Phys.* **37** 41

[38] Petrov I D, Sukhorukov V L, Leber E, and Hotop H 2000 *Eur. Phys. J. D* **10** 53

[39] Gopalan A, Leber E, Bömmels J, Paul S P H, Allegrini M, Ruf M-W, and Hotop H 2004 *Eur. Phys. J. D* **30** 163

[40] Bömmels J, Leber E, Gopalan A, Weber J M, Barsotti S, Ruf M-W, and Hotop H 2001 *Rev. Sci. Instrum.* **72** 4098

[41] Smith D and Spanel P 1994 *Adv. At. Mol. Opt. Phys.* **32** 307

[42] Walter C W, Lindsay B G, Smith K A, and Dunning F B 1989 *Chem. Phys. Lett.* **154** 409

[43] Miller D R 1988 *Atomic and Molecular Beam Methods* ed G Scoles (New York: Oxford University Press)

[44] Braun M, Barsotti S, Marienfeld S, Leber E, Weber J M, Ruf M-W, and Hotop H 2005 *Eur. Phys. J. D* **35** 177

[45] Braun M, Ruf M-W, Hotop H, and Allan M 2006 *Chem. Phys. Lett.* **419** 517

[46] Datskos D G, Christophorou L G, and Carter J G 1992 *J. Chem. Phys.* **97** 9031

[47] Wentworth W E, George R, and Keith H 1969 *J. Chem. Phys.* **51** 1791

[48] Petrovic Z L and Crompton R W 1987 *J. Phys. B: At. Mol. Phys.* **20** 5557

[49] Alge E, Adams N G, and Smith D 1984 *J. Phys. B: At. Mol. Phys.* **17** 3827

[50] Levy R G, Burns S J, and McFadden D L 1994 *Chem. Phys. Lett.* **231** 132